Coronal heating by collision and cancellation of magnetic elements

D. W. Longcope and C. C. Kankelborg
Department of Physics, Montana State University,
Bozeman, MT 59717

Received ________________; accepted ________________

Submitted to *Astrophysical Journal*

ABSTRACT

A model is proposed for the coronal response to the interaction between randomly moving photospheric magnetic flux elements. In this model the collision between two elements of opposing sign results in reconnection and the appearance of an X-ray bright point. A section of quiet sun on which elements are distributed and moving randomly, will contain a number of X-ray bright points. The model combines a distribution of element sizes, random velocities of the elements, and a model for a pair-wise collisions. This results in quantitative predictions for surface density of X-ray bright points, the distribution of their luminosities, and their contribution to the total heat flux in the quiet sun. The predictions depend principally on the densities of flux elements of each sign $\bar{B}_+$ and $\bar{B}_-$, the average element size $\bar{\Phi}$, and the random velocity v_0. The predicted heat flux, $F_{\rm XBP} = 0.1\,\bar{B}_+\bar{B}_-v_0$, is in rough agreement with published observational studies of X-ray bright points but well below the flux required to supply heat to the quiet sun corona. Other predictions of the model are similarly consistent with published studies.

Subject headings: Sun: corona – Sun:magnetic fields – Sun: X-rays, gamma rays

1. Introduction

The Sun and most other late main-sequence stars have hot outer coronae detectable by their emission of X-rays. These coronae are thought to result from plasma heating related somehow to the combination of magnetic fields and convective envelopes present on these astrophysical objects. The magnetic field is believed to contribute either by transmitting mechanical wave energy upward (Hollweg 1990) or by slowly storing and then rapidly releasing stress (Parker 1988). In the second mechanism, called *nanoflaring*, the storage and release is thought to resemble similar processes observed in flares and microflares. Indeed, flares and microflares are assumed to constitute the high energy portion of a continuum of events extending to much lower, as yet unobservable energies – nanoflares. Flares and microflares occur at rates which scale inversely with their energies (Lin *et al.* 1984, Dennis 1985); if this trend continues to lower energies then the entire range would provide a source of effectively continuous heating. Extrapolation of observed values yields a total heating power due to nanoflares somewhat lower than needed to explain the presence of the corona (Hudson 1991).

Flares, microflares and nanoflares undoubtedly deposit heat in the corona even though it is not clear whether they are the dominant coronal heating source. The basic understanding of these phenomena is that plasma motions in the convection zone stress the coronal field and the field relaxes occasionally through *magnetic reconnection*. While this general description explains many observed features of individual flares and microflares it has taken some time to formulate a quantitative model based on it. One major obstacle is that magnetic reconnection is understood so poorly that there is no accepted model of how much heating it might generate. Recently Longcope (1996) introduced the *minimum current corona* (MCC) model which placed a lower bound on reconnection energetics. It does so by assuming quasi-static processes involving discrete photospheric elements. The model has been applied to an individual flare with some success (Longcope and Silva 1998). In principle, it may be applied to a theoretical ensemble of active regions to calculate an average heating rate. The present work will attempt such a calculation, but for the quiet Sun.

Magnetic reconnection is also believed to occur in quiet Sun regions where it gives rise to features known as X-ray bright points (XBPs). These are localized regions of coronal brightening apparently caused by the interaction of two photospheric magnetic elements. According to present models the heating is caused by magnetic reconnection around the interacting elements (Priest *et al.* 1994, Longcope 1998). As with nanoflares, the continual occurrence of XBPs will serve as a source of heating for the quiet Sun corona. While the quiet Sun is not as bright as an active region it still contains coronal material whose existence demands some source of heating. The amount of heating required to maintain the quiet sun corona has been calculated to be $3 \times 10^5\,\mathrm{erg\,sec^{-1}\,cm^{-2}}$ (Withbroe and Noyes 1977), some 30 times less than required in active regions.

Habbal and Grace (1991) measured the radiative losses by XBPs (which they identify as that portion of the transition region characterized by temporal fluctuation) in the quiet sun to be only $5 \times 10^4\,\mathrm{erg\,sec^{-1}\,cm^{-2}}$. Since this is almost an order of magnitude lower than required, it would seem that XBPs are not the dominant heating source in the quiet sun corona any more than nanoflares are in the active corona. Nevertheless, XBPs do provide a source of heating to the quiet sun, and this work develops a theoretical model to quantify it.

The magnetic field of the photosphere consists of isolated magnetic elements which move under the influence of complex flows (Schrijver *et al.* 1996, Schrijver *et al.* 1998). A given quiet Sun region contains elements of both signs and a wide range of magnetic fluxes Φ. Within a surface area A the average number of positive elements with fluxes in the range $(\Phi, \Phi + d\Phi)$ is given by the distribution function $N_+(\Phi)\,A\,d\Phi$. Collisions between pairs of elements result in complete or partial cancellation (between opposing signs) or coalescence into a single larger element (between like signs). The destruction of flux through cancellation is balanced by creation through flux emergence, as ephemeral active regions. Schrijver *et al.* (1997a) formulated a model they called *magneto-chemistry* for the evolution of the distribution functions, $N_\pm(\Phi)$, under the action of cancellation, coalescence and emergence.

X-ray bright points appear to be associated primarily with the cancellation events; collisions between opposing flux elements (Webb *et al.* 1993, Harvey *et al.* 1994). The collision of the photospheric elements is accompanied by magnetic reconnection in the corona. There may also be reconnection in the chromosphere or below, and this would undoubtedly have energetic consequences. Nevertheless, the present work will concern only the coronal field and the heating due to its reconnection.

During such a collision, the coronal field lines from each element must be disconnected from the background field and connected to one another. If this is done in the absence of a plasma, for example in a vacuum, no energy is dissipated. The re-mapping of magnetic field lines does not, however, occur so readily in the highly conducting corona. The prevailing belief holds that flares, microflares, and XBPs, result from a sudden burst of reconnection – the field lines seem to be re-mapped all at once. The MCC models the energy of reconnection as the difference in energies between the *equilibrium* magnetic fields before and after the re-mapping (reconnection) occurs. Since it uses only equilibrium fields the MCC is a *quasi-static* model.

Application of the MCC model to a two element collision has provided an estimate of the energy released by reconnection in this event (Longcope 1998). This energy depends on the fluxes of the colliding elements but not on the velocity of their collision. In this work we will estimate the average heating rate from the distribution functions $N_\pm(\Phi)$, the rates of pair-wise collision, and the energy released per collision. The next section describes the model of photospheric flux elements, their distributions, motions and the energy released by their collision. In §3 these are combined to calculate the theoretical heat flux and the surface density of XBPs as a function of luminosity. The model presented in §2 assumes a uniform distribution of elements on the solar surface, rather than a distribution concentrated along the magnetic network. Section 4 estimates the effect of the magnetic network to be a factor of 2 enhancement in the heat flux above that from §3. In §5 the results of the model are placed in the context of published XBP studies. No study to date provides all of the measurements necessary to definitively test the model. Making plausible assumptions, however, it is possible to show that the model is in rough agreement with the existing body of observational work. Finally, §6 discusses the implications of this model for our understanding of the corona.

2. The model

2.1. Flux elements

The distribution functions for each polarity $N_{\pm}(\Phi)$ have been measured in quiet Sun (Schrijver *et al.* 1996, Schrijver *et al.* 1997c) and plage regions (Schrijver *et al.* 1997b). The most accurate measurements, using the Michaelson Doppler Interferometer (MDI) on board SOHO, show the distribution functions in the quiet Sun to be approximately exponential (Schrijver *et al.* 1997c)

$$N_{\pm}(\Phi) = \beta^2 \, \bar{B}_{\pm} \, e^{-\beta\Phi} \quad , \tag{1}$$

over the range $2 \times 10^{18}\,\mathrm{Mx} \lesssim \Phi \lesssim 20 \times 10^{18}$ Mx. The parameters of the exponential are found from a best fit of measured histograms to expression (1). Schrijver *et al.* find $\beta \simeq 0.3 \times 10^{-18}$ and $\bar{B}_{\pm} \simeq 1.6$ G for their quiet Sun observations. The first of the fit parameters relates to the average flux of an element

$$\langle\Phi\rangle \;\equiv\; \bar{\Phi} \;=\; 1/\beta \;\simeq\; 3 \times 10^{18}\,\mathrm{Mx} \quad . \tag{2}$$

The second gives the mean flux density for each sign defined by the moment

$$\bar{B}_{\pm} \equiv \int_0^{\infty} \Phi \, N_{\pm}(\Phi) \, d\Phi \quad . \tag{3}$$

The quiet sun has little net flux $\langle B_z \rangle = \bar{B}_{+} - \bar{B}_{-}$, so the mean values for each sign are roughly equal $\bar{B}_{+} \simeq \bar{B}_{-}$. The density of all poles per unit area is $n_{\pm} \equiv \beta\bar{B}_{\pm} = 4.8 \times 10^{-3}\,\mathrm{Mm}^{-2}$. (This is 10 poles, of each sign, in a field of view one arcminute square, near disk center).

The magneto-chemistry equations, introduced by Schrijver *et al.* (1997a), yield expression (1) as an approximate steady state under the actions of collisions, destruction and creation. In this steady state the constants β and $\bar{B}_{\pm}$ depend on the rates of creation and collision, which appear as parameters of the model. For our purposes, however, it will suffice to use (1) based on its approximation of observed data, and to take the values of β and $\bar{B}_{\pm}$ from these measurements.

The spatial distribution of magnetic elements is more complex than their size distribution. Photospheric flows rapidly sweep the elements to supergranule boundaries on which subsequent motions then occur. At any instant, therefore, the spatial distribution of elements will be concentrated along the supergranule boundaries, forming what is known as the magnetic network.

To begin with we will neglect the complexities implied by the network and model the spatial distribution of each species to be uniform and independent of the other; that is to say, the elements will be distributed as Poisson point processes (Kendall and Moran 1963). Figure 1 shows a realization of this type. Elements are distributed randomly over a 300 Mm $\times$ 150 Mm region of the quiet Sun. Positive and negative elements are shown as white and black respectively, with the flux of an element represented by its area. The distribution of fluxes are governed by (1) with $\beta = 0.3 \times 10^{-18}\,\mathrm{Mx}^{-1}$ and $\bar{B}_{\pm} = 1.6$ G.

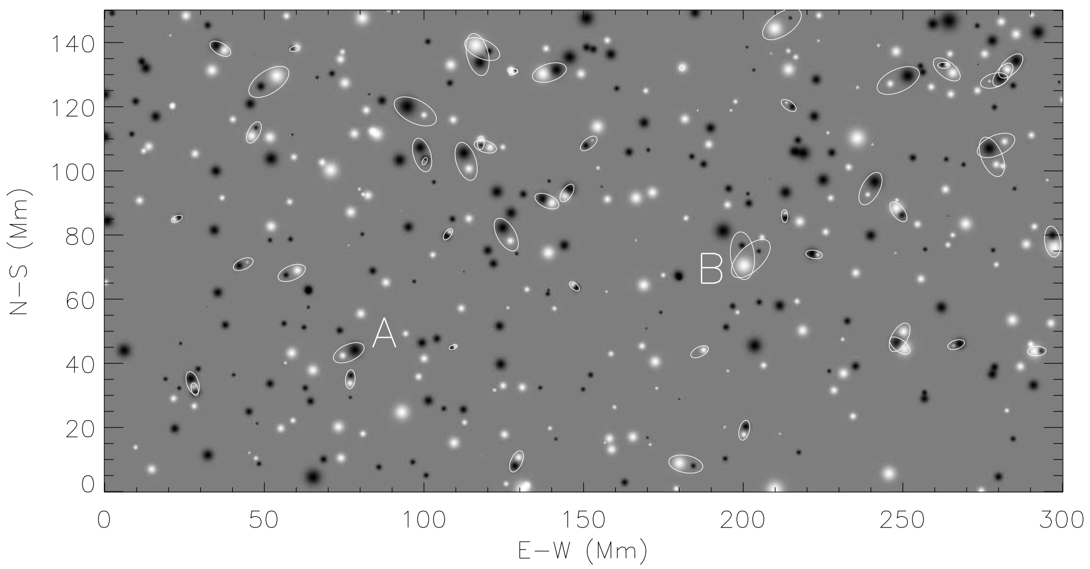

Fig. 1.— An illustration of uniformly distributed flux elements with exponentially distributed fluxes. Pairs which are colliding (using $B_0 = 30$ G) are circled in white. A depicts a typical binary collision, while B depicts a more complex (three-body) interaction. Of the 55 pairs in the figure 34 are binary collisions.

In §4 we will relax the assumption of spatial uniformity, introducing a modified model with elements concentrated along a magnetic network. This will enhance the heat flux by a constant factor related to the size of the networks cells. A uniform distribution turns out to be accurate in the limit limit of small cells. Furthermore, assuming a Poisson point processes results in a simpler model from which more results can be extracted analytically. Therefore we do our initial analysis for this case.

The flux elements are buffeted by the turbulent photospheric flows causing them to move randomly. Schrijver *et al.* (1996) find the typical root-mean-squared (rms) velocity to be ~ 200 m/sec. They also find that the rms velocity decreases slightly with increasing flux. To simplify our model we introduce the flux-dependence through a power-law relationship

$$v_{\rm rms}(\Phi) \;=\; v_0\,(\beta\Phi)^{-\nu} \quad , \tag{4}$$

so that $v_0 \simeq 200\,{\rm m/sec}$ is the velocity of the typical element ($\Phi = \bar{\Phi} = 3 \times 10^{18}$ Mx). We will leave the exponent ν unspecified to explore the effect of the flux-dependent velocity; it will turn out to have little effect on most results. The rather weak dependence observed by Schrijver *et al.* suggests a value near zero. In §5 we will consider a more accurate model of $v_{\rm rms}(\Phi)$ by combining two terms of type (4).

2.2. Collisions

Magnetochemistry concerns the *photospheric* magnetic field and the collisions between photospheric elements. These collisions occur when the observed features approach one another and then disappear from the magnetogram. In one interpretation (Zwaan 1987) this represents a flux tube being submerged below the photosphere. The present work, however, concerns the coronal magnetic field *above* the photosphere. Above the discrete photospheric features the magnetic field is believed to expand to fill the entire volume of the corona (Gabriel 1976). A *collision*, as we will use the term, occurs when two opposing magnetic elements approach close enough that their coronal field begins to interact. Because of their drastic expansion, fields in the corona will interact well before they do in the photosphere. The reconnection energy which will concern us relates to the interaction of these coronal fields, and not to any process in the photosphere or chromosphere.

The MCC concerns magnetic geometry alone, and the term "corona" refers to that region above the canopy, where the magnetic field has fully expanded. In actual fact, this point may be characterized by temperatures lower than those associated with the corona. Thus the process of magnetic reconnection described by the MCC model may lead to signatures in coronal, transition region and possibly chromospheric spectral lines. Most of the reconnection does occur in the genuine solar corona, thereby leading to coronal bright points. Bearing this in mind we will distinguish between confined and unconfined magnetic fields with the terms "photospheric" and "coronal" respectively.

A single collision between two features was described and modeled by Longcope (1998). Prior to encountering one another each magnetic feature is connected, through its coronal field lines, to "external" sources of flux which we will call the *background* field. This is to say, if they do not connect to one another the elements must connect elsewhere. The background field will be different for each collision, depending as it does on all the "spectator" elements in the immediate vicinity. A simple example of a background is a uniform horizontal field with strength B_0. The background field is taken to be uniform only in comparison to the fields of the interacting poles, and will presumably differ in direction and and magnitude, for each colliding pair. With respect to the orientation of the colliding pair (i.e. from P to N) all background field directions will be equally likely, since bipole orientations themselves will be distributed uniformly. Quantities characterizing collisions will, therefore, reflect an average over all background field directions. We will assume, however, that a single choice of field strength B_0 can serve as a proxy for the influence of external sources on the typical collision.

The background field strength B_0 is an extremely important quantity in the theory of collisions since without it there would be no collisions: the features would be completely connected to one another at arbitrary separation. As a result all quantities related to collisions depend on B_0. We will assume that all collisions are governed by a single parameter B_0, which we will take to lie in the range $10\,\mathrm{G} \lesssim B_0 \lesssim 100\,\mathrm{G}$ typical of the lowest corona. For estimates we will use the intermediate value $B_0 = 30$ G. This occurs, for example, within $100,000$ km of a moderate active region. In the end B_0 is best treated as a parameter of the model which may be determined by fitting to observational data. Doing so in §5 will show $B_0 = 30$ G to give reasonably good agreement.

Prior to collision, all field lines from each element join the background field. These field lines fill a zone extending $\sim \sqrt{\Phi/B_0}$ from each element, and extending indefinitely "downwind", along the background field direction (Longcope 1998). The two elements will first encounter one another when their zones overlap; this occurs at a separation (Longcope 1998)

$$d(\Phi_+,\Phi_-) \;=\; \tfrac{1}{2}B_0^{-1/2}\,(\,\Phi_+^{1/2} \,+\, \Phi_-^{1/2}\,) \quad . \tag{5}$$

The actual distance of first encounter depends on the orientation of the pair relative to the background field. Since poles precisely "downwind" of one another can interact at distances greatly exceeding (5), the interaction region is not circular. Nevertheless, energetically significant reconnection will occur only between poles separated by distances

$\sim d(\Phi_+, \Phi_-)$ regardless of their orientation; more distant interactions result in little power dissipation (Longcope 1998). For this reason we will adopt a circular interaction region. Expression (5) for the interaction radius depends principally on the larger of the two fluxes $\Phi_> \equiv \max(\Phi_+, \Phi-)$, and will be simplified further using its upper bound

$$d(\Phi_+, \Phi-) \ \leq \ D(\Phi_+, \Phi-) \ = \ B_0^{-1/2} \Phi_>^{1/2} \quad . \tag{6}$$

For the typical choices $B_0 = 30$ G and $\Phi_> = \bar{\Phi} = 3 \times 10^{18}$ Mx, this gives an interaction distance of 3 Mm or $4''$. We shall assume that each pair of elements separated by less than D are colliding, regardless of their orientation. In fig. 1 those pairs of elements involved in collisions are circled.

The model of Longcope (1998) concerns collisions between only two elements at a time. We will apply the results of this pair-wise model to each colliding pair in a given distribution. This is obviously correct for two elements each involved in a collision only with the other (such as the pair labeled A in fig. 1). There will, however, be instances where one elements has more than one opposing pole within the interaction distance $D(\Phi_+, \Phi_-)$ at a single time (such as the positive pole labeled B in fig. 1). It is likely that reconnection in such a circumstance is more complex than in the pair-wise case. No model yet exists for such cases, so we will neglect any possible complications and apply the binary model to each pair independently (i.e. B counts as two different collisions). It turns out that multiple collisions are a minority of collisions so this approximation is reasonable; 34 of the 55 pairs are binary collisions in fig. 1. The error incurred by approximating the remaining interactions as 21 pairs, rather than a smaller number of more complex interactions, cannot even be estimated since no quantitative model exists for the more complex interactions.

To estimate the rarity of multiple collsions consider the *average* number of opposing elements Φ_- within a radius $D(\Phi_+, \Phi_-)$ of a given element Φ_+,

$$\begin{aligned} f(\Phi_+) \ &\equiv \ \pi B_0^{-1} \left(\Phi_+ \int_0^{\Phi_+} N_-(\Phi_-)\, d\Phi_- \ + \ \int_{\Phi_+}^{\infty} \Phi_- N_-(\Phi_-)\, d\Phi_- \right) \\ &= \ \frac{\pi \bar{B}_-}{B_0} \left(\beta\Phi_+ \ + \ e^{-\beta\Phi_+} \right) \quad . \end{aligned} \tag{7}$$

The actual number of collisions suffered by the flux element Φ_+ is a Poisson variable whose mean is f. The factor $\xi_- \equiv \pi \bar{B}_-/B_0$ in expression (7) is a dimensionless quantity characterizing the rarity of collisions. As long as $\xi_- \ll 1$ then for the majority of positive poles, say those for which $\beta\Phi_+ \leq 3$, only a small fraction ($\sim \xi_-$) will be involved in binary collisions, while a much smaller fraction still ($\sim \xi_-^2$) will be involved in multiple collisions. The parameters used in fig. 1 give values $\xi_+ = \xi_- = 0.17$ and Poisson statistics predict 63% of the collisions will be binary, consistent with the fraction $34/55 \simeq 0.62$ from the example.

The rate at which a given element Φ_+ collides with opposing elements with fluxes in the range $(\Phi_-, \Phi_- + d\Phi_-)$, will be written as $r(\Phi_+, \Phi_-)N_-(\Phi)\, d\Phi_-$. The function $r(\Phi_+, \Phi_-)$ will depend on the "cross-section" for collisions, $D(\Phi_+, \Phi_-)$ and on the relative velocities of the elements. In particular the rate is proportional to the rms of that component of the relative velocity along the line of separation — the radial component. Assuming the motion of the two colliding elements to be independent the rms relative radial velocity of the pair is

$$v_{\rm rr}(\Phi_+, \Phi_-) \;=\; \langle [\hat{\mathbf{r}} \cdot (\mathbf{v}_+ - \mathbf{v}_-)]^2 \rangle^{1/2} \;=\; \left[\tfrac{1}{2} v_{\rm rms}^2(\Phi_+) \;+\; \tfrac{1}{2} v_{\rm rms}^2(\Phi_-) \right]^{1/2} \quad . \tag{8}$$

This expression is dominated by the larger of the two velocities which is that of the smaller flux. To simplify the expression we introduce its upper bound

$$v_{\rm rr}(\Phi_+, \Phi_-) \;\le\; V(\Phi_+, \Phi_-) \;\equiv\; v_0 \beta^{-\nu}\, \Phi_<^{-\nu} \quad , \tag{9}$$

where $\Phi_< \equiv \min(\Phi_+, \Phi_-)$ is the smaller flux. The collision coefficient r is the flux of opposing elements through the circle of interaction. Approximating r by its upper bound yields

$$r(\Phi_+, \Phi_-) \;\simeq\; \pi D(\Phi_+, \Phi_-)\, V(\Phi_+, \Phi_-) \;=\; \pi\, v_0 B_0^{-1/2} \beta^{-\nu}\, \Phi_<^{-\nu}\, \Phi_>^{1/2} \quad . \tag{10}$$

For collisions between elements $\Phi_+ = \Phi_- = \bar{\Phi}$ we find a rate coefficient $r(\bar{\Phi}, \bar{\Phi}) = \pi v_0 (B_0 \beta)^{-1/2} \simeq 2 \times 10^{13}\,\mathrm{cm^2/sec}$, a number similar to the coefficient for photospheric collisions found by Schrijver *et al.* (1997a).

2.3. Collision energetics

Once initiated a collision may proceed to a complete or partial cancellation of the photospheric elements or progress as a grazing encounter whereby the elements simply "brush" past one another. Either case involves a transfer of coronal flux generically called *reconnection*. As the elements approach each other their field lines are disconnected from external partners and joined to one another (see fig. 2). In the process there is a transfer of flux across a field line known as the separator. In the case of complete cancellation this flux transfer proceeds until the two elements are completely connected to each other. At this point, since the pair is completely decoupled from the background field, it may be subducted below the surface. Only the final subduction is identified as a "collision" by Schrijver *et al.* (1997a); we consider the entire flux-transfer process to be a collision, ignoring the subduction.

In a grazing encounter flux is first transfered into the bipole and then back out. In the end the two poles are once again decoupled from one another and resume uncoupled

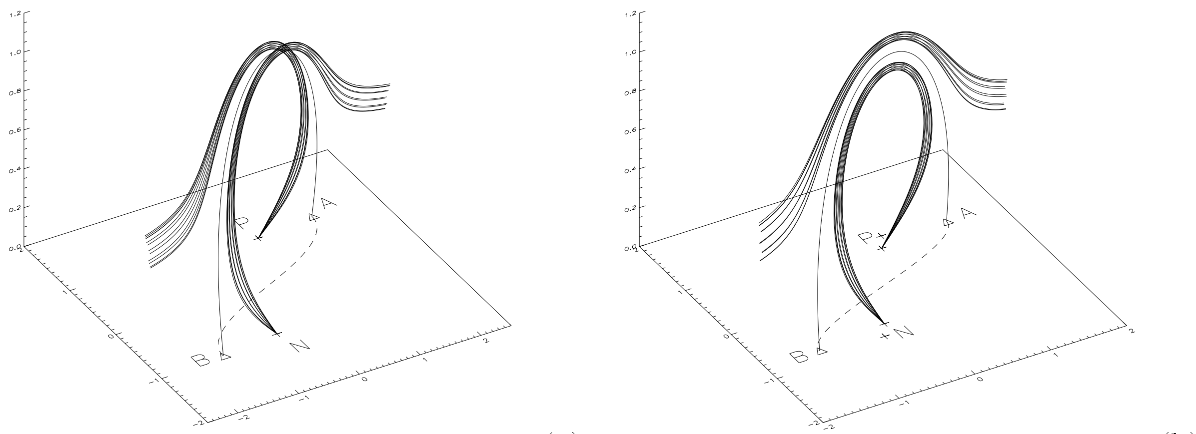

(a) (b)

Fig. 2.— A step in the reconnection of the flux elements P and N. (a) Bundles of field lines connect each element to the horizontal background field. (b) The elements approach slightly (previous positions are also marked with +'s) and these the field lines are forced to reconnect. This leaves a loop connecting P to N and an essentially horizontal external field. The process of reconnection forces additional flux through the separator loop, shown connecting points A and B. Such a change in flux requires an electric field by Faraday's law.

evolution. Like the cancellation event, this encounter involves the transfer of coronal flux and therefore constitutes a collision in our use of the term. Since the photospheric flux elements do not contact, it is *not* a collision in the magneto-chemistry model. On the other hand, the encounter of like-signed photospheric elements does not lead to flux transfer (the elements cannot share flux since they have the same sign) and thus is *not* a collision in our model. Nor is there much observational evidence for energy released by such encounters; rather XBPs are almost always associated with elements of opposite polarities (Webb *et al.* 1993, Harvey *et al.* 1994).

The coronal response to a collision results from the magnetic reconnection. Transferring flux across the separator requires an electric field by Faraday's law (Longcope and Cowley 1996). The corona is highly conductive and will not permit an electric field under ordinary circumstances. Fast magnetic reconnection occurs when extra-ordinary circumstances create a significant electric field. One possible extra-ordinary circumstance is for a current sheet to trigger some form of plasma instability thereby enhancing the effective collision rate (Longcope and Cowley 1996, Longcope 1996). In such a scenario the flux-transfer electric field occurs in the presence of a current, implying electromagnetic work.

The work done in transferring fluxes is the source of heating we will include in our model. The work can be estimated by the difference between energies of equilibrium magnetic fields before and after reconnection; this estimate is a lower bound on the energy. In this estimate the energy released does *not* depend on the resistivity or any details of the reconnection. In particular, it does not depend on rates of motion, or the photospheric velocity. This is a natural characteristic of a quasi-static heating model (Longcope 1996); it results from neglecting all possible dynamical contributions such as Alfvén waves. These potentially significant effects are neglected in order to quantitatively assess their significance.

Longcope (1998) considered collisions between equal fluxes, $\Phi_+ = \Phi_- = \Phi$, and found that complete cancellation released an energy

$$\mathcal{E} \;=\; \alpha\, B_0^{1/2} \Phi^{3/2} \quad , \tag{11}$$

where α is a dimensionless coefficient. The MCC contains a single free parameter, θ, describing the threshold for whichever plasma instability is actually responsible for reconnection. For a low value of θ reconnection occurs readily; $\theta = 0$ corresponds to a vacuum. For the case of equal fluxes Longcope found $\alpha = 0.035\theta$. Apart from the factor α, expression (11) follows from dimensional considerations alone: the only physically relevant parameters in a quasi-static process are the fluxes and the background field.

Figure 3 presents an example of a series of reconnection events occurring during the complete cancellation of two poles. The poles each have flux $\Phi = \bar{\Phi} = 3 \times 10^{18}$ Mx, and are moving toward one another at 100 m/sec in the presence of a $B_0 = 30$ G background field. The elements first encounter each other at $t = 0$ and have cancelled ~ 4 hours later. In fig. 3a the flux connecting the two poles (solid) increases from zero to 3×10^{18} Mx. It changes in a series of reconnection events (vertical segments) between which it is held constant (horizontal segments) by the highly conducting corona. The dotted line shows the hypothetical evolution in the absence of the corona (i.e. $\theta = 0$). The reconnection events are triggered when the coronal current has exceeded a threshold (the threshold parameter here is $\theta = 0.25$). The free-energy stored in the coronal current, shown in fig. 3b, builds up slowly and drops abruptly with each reconnection event. This energy drop is the source of dissipated heat in the corona. Figure 3c shows the impulsive heating events felt by the coronal plasma. Roughly ten such heating events, each of $\Delta\mathcal{E} \sim 2 \times 10^{25}$ ergs, have occured by the end of the 4 hour cancellation. Thus the complete cancellation produces $\sim 2 \times 10^{26}$ ergs of heating, in agreement with expression (11).

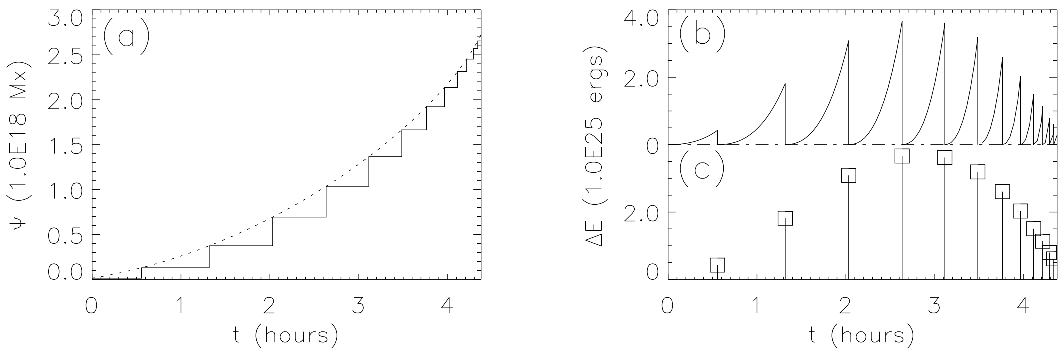

Fig. 3.— The collision and cancellation of two magnetic poles. (a) The flux interconnecting the poles (solid), in units of 10^{18} Mx. In the absence of a corona the flux would follow the dotted line. (b) The free energy stored in the coronal current, in units of 10^{25} ergs. (c) The impulsive energy releases resulting from the reconnection events

Longcope (1998) considered encounters between equal fluxes $\Phi_+ = \Phi_-$. In the present work, however, we must also include collisions between unmatched fluxes: $\Phi_+ \neq \Phi_-$. An application of the MCC to this wider class of events is not yet complete, but it is possible to derive approximate expressions based on scaling arguments. In the MCC model heating energy results from a simple inductive drive transfering flux $\Delta\Phi$ in the presence of current I: $\mathcal{E} \sim c^{-1} I \, \Delta\Phi$. The total flux transfered will be dictated by the smaller of the two elements: $\Delta\Phi \simeq \Phi_<$. The flux is transfered in small pieces, each in the presence of a current I assumed to be the maximum current admissible before reconnection is triggered. By hypothesis this threshold current must depend on aspects of the magnetic field other than the inductively driven current itself. In other words it must depend on geometry and strength of the field around the separator, dictated primarily by interaction of the background field with the the larger flux element. Dimensional arguments thus lead to a threshold current $I \sim c\sqrt{B_0\Phi_>}$. Physically this is an inductive current $I \sim c^{-1}\Phi_>/\mathcal{L}$, where $\mathcal{L} \sim c^{-2}D$ is the self-inductance of the separator of length $\sim D$.

The scaling arguments above review the basic physics of the MCC calculation applied to equal flux elements. In addition, these arguments identify the different contributions made by each of a mismatched pair of flux elements. Combining these contributions and retaining eq. (11) for the special case $\Phi_+ = \Phi_- = \Phi$ leads to the expression

$$\mathcal{E}(\Phi_+, \Phi_-) \;=\; \alpha B_0^{1/2}\Phi_>^{1/2}\,\Phi_< \quad . \tag{12}$$

We will use this simple expression, with $\alpha = 0.035\,\theta$, for all manner of collisions. θ will remain as a free parameter descibing the efficiency of fast magnetic reconnection.

After initiation, a collision will last as long as it takes the elements to cancel or to brush past one another. Their initial separation $D(\Phi_+, \Phi_-)$ and their relative velocities $V(\Phi_+, \Phi_-)$ lead to an estimate for the lifetime of a head-on collision

$$\tau_{\rm life}(\Phi_+, \Phi_-) \;\simeq\; \frac{D(\Phi_+, \Phi_-)}{V(\Phi_+, \Phi_-)} \;=\; v_0^{-1}B_0^{-1/2}\beta^{\nu}\,\Phi_>^{1/2}\,\Phi_<^{\nu} \quad . \tag{13}$$

In the collision in fig. 3 the poles are moving with a relative velocity of 200 m/sec $\simeq v_0$. The collision lasts for $\simeq 4$ hours, in agreement with eq. (13).

Expressions (12) and (13) are motivated by simple head-on collisions, however, a simple model shows them to be good approximations for grazing encounters as well. In a head-on collision the pole separation decreases from maximum, D, to zero, while in a grazing encounter the separation first decreases and then increases again. In a head-on collision, the "distance" traveled by the incident pole (i.e. motion relative to a stationary pole) is exactly D. Consider a grazing path to be a straight line (a chord) through a circle of radius D. Passing to within an impact-parameter $h \le D$ of the center, the path length is $2\sqrt{D^2 - h^2}$. Assuming all impact parameters to be equally likely, the the average path length for a grazing is $\frac{1}{2}\pi D$. This implies the average lifetime of a grazing encounter will be $\sim 60\%$ longer than a collision. The average lifetime for the set of collisions and grazes will be somewhere in between.

Heating energy from an encounter can be calculated as the integral of a velocity-independent force (Longcope 1998) along the path of relative motion. Since this force is largest at small separations its contribution in grazing encounters will be systematically smaller. This smaller force is compensated by longer paths to give an energy $\mathcal{E}$ for grazing encounters comparable to expression (12) for collisions. Using the approximate force law force $\mathbf{F} = 2\mathcal{E}_0(d-r)d^{-2}\,\hat{\mathbf{r}}$ where $\mathcal{E}_0$ is the energy released in a head-on collision (i.e. eq.. [12]), leads to an average energy release $\frac{2}{3}\mathcal{E}_0$ for grazing encounters. Applying these expression to both kinds of encounters will introduce an error no larger than 50% in the end result. Thus we will henceforth refer to all encounters, even grazing encounters, by the term "collision", and use expressions (12) and (13) for their energy release and life-time respectively.

In a collision the energy $\mathcal{E}$ (eq. [12]) is released over the life-time $\tau_{\rm life}$ through a series of impulsive events (see fig. 3c). Smoothing over the impulses leads to an average power dissipation

$$\bar{\mathcal{P}}(\Phi_+,\Phi_-) \;=\; \frac{\mathcal{E}(\Phi_+,\Phi_-)}{\tau_{\rm life}(\Phi_+,\Phi_-)} \;=\; \bar{\mathcal{P}}_0\,(\beta\Phi_<)^{1-\nu} \quad , \tag{14}$$

where $\bar{\mathcal{P}}_0 \equiv \alpha B_0 v_0 \bar{\Phi} \simeq 0.6\,\theta\,10^{23}\,\mathrm{erg/sec}$. This predicts a power of $\bar{\mathcal{P}} \sim 1.6\times10^{22}\,\mathrm{erg/sec}$ in fig. 3, consistent with the series of $\sim 2\times10^{25}$ erg impulses occurring every ~ 20 minutes.

Our complete model consists of one XBP located at each reconnection site, releasing an average power (14). Figure 4 is an image of the power liberated by reconnection in the 55 colliding pairs in fig. 1. The emitted power, given by expression (14) with $\nu = \frac{1}{4}$, is distributed as a Gaussian whose half-width contour is the same ellipse which encircles the pair in fig. 1. The resulting map is then convolved with a Gaussian point-spread-function of width $2\rlap{.}''5$ to simulate instrumental resolution. Black corresponds to high intensity, white to no emission. In what follows we will compute the power and related statistics of these reconnection events.

3. Statistics of reconnection events

3.1. Heat flux

The ingredients above can be combined to yield the statistics of the reconnection events in a model of the quiet sun. One event occurs with each collision, releasing an energy $\mathcal{E}(\Phi_+,\Phi_-)$. The total heat flux generated by the events is

$$\begin{aligned} F_{\rm XBP} &= \int_0^\infty d\Phi_+ \int_0^\infty d\Phi_-\; \mathcal{E}(\Phi_+,\Phi_-)\, r(\Phi_+,\Phi_-)\, N_+(\Phi_+)\, N_-(\Phi_-) \\ &= \pi C_\nu\, \alpha\, \bar{B}_-\bar{B}_+ v_0 \quad . \end{aligned} \tag{15}$$

The dimensionless coefficient C_ν, from performing the double integral

$$C_\nu \equiv 2^\nu(1-\tfrac{1}{4}\nu)\Gamma(2-\nu) \quad , \tag{16}$$

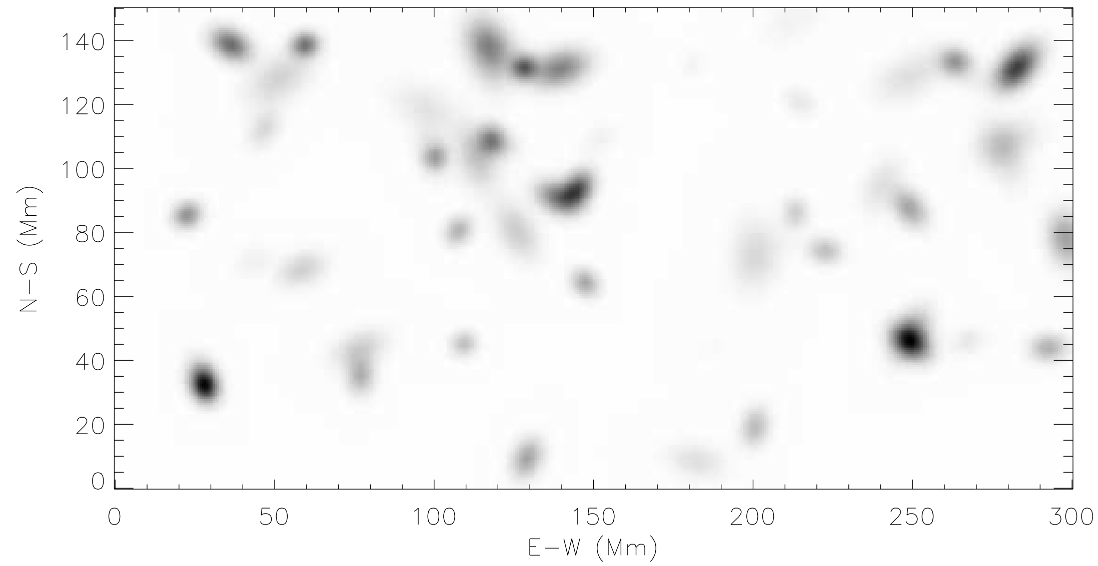

Fig. 4.— An image of the emission from those bipole collisions shown in fig. 1. The image uses a reverse grey-scale in which black represents high intensity. The image has been blurred to simulate an instrumental resolution of $2''\!.5$.

varies smoothly between $C_0 = 1$ and $C_1 = 3/2$. Taking the value $\nu = 0$ we find that

$$F_{\rm XBP} \simeq \theta\, 0.1 \bar{B}_- \bar{B}_+ v_0 \simeq 0.5\,\theta\, 10^4\,{\rm ergs\,sec^{-1}\,cm^{-2}} \tag{17}$$

for the typical choices of $\bar{B}_\pm = 1.6$ G and $v_0 = 2 \times 10^4$ cm/sec. Note that the external field strength B_0, while important for the theory of collisions, does not enter the total heat flux (except for the assumption that $\bar{B}_\pm \ll B_0$ for dominant binary collisions). Furthermore, when the velocity exponent ν is unity, and the smallest elements are moving much faster than those typically observed, the heat flux is only larger by 50%.

3.2. Event spectrum

The number of reconnection events at a given time is the production rate of events times the lifetime of events. The number per density of each species is

$$r(\Phi_+, \Phi_-)\tau_{\rm life}(\Phi_+, \Phi_-) = \pi D^2(\Phi_+, \Phi_-) \ \ ,$$

which matches the area of interaction for the pair. The surface density of reconnection events is therefore

$$\mathcal{D}_0 = \pi \int_0^\infty d\Phi_+ \int_0^\infty d\Phi_- \, D^2(\Phi_+, \Phi_-)\, N_+(\Phi_+)\, N_-(\Phi_+) \;=\; \frac{3\pi \bar{B}_+ \bar{B}_-}{2B_0\bar{\Phi}} \quad . \tag{18}$$

For typical parameters this predicts 2.3 in a field of view one arc-minute square, near disk center.

The number of such events within a range of powers $(P, P+dP)$ is given by a spectral density $\mathcal{N}(P)\,dP$. This spectral density is calculated by restricting the count in (18) to a shell of specified power,

$$\begin{aligned} \mathcal{N}(P) &= \pi \int_0^\infty d\Phi_+ \int_0^\infty d\Phi_- \, D^2(\Phi_+, \Phi_-)\, N_+(\Phi_+)\, N_-(\Phi_-)\, \delta[\, P - \bar{\mathcal{P}}(\Phi_+, \Phi_-)\,] \\ &= \frac{2\pi\mu \bar{B}_+ \bar{B}_-}{\bar{\Phi} B_0 \bar{\mathcal{P}}_0} \left\{ \left(\frac{P}{\bar{\mathcal{P}}_0}\right)^{\mu-1} + \left(\frac{P}{\bar{\mathcal{P}}_0}\right)^{2\mu-1} \right\} \exp\!\left[-2\left(\frac{P}{\bar{\mathcal{P}}_0}\right)^{\mu} \right] \quad , \end{aligned} \tag{19}$$

and the exponent $\mu = 1/(1-\nu)$. The spectral density becomes highly localized around $P = \bar{\mathcal{P}}_0$ as $\nu \to 1$ ($\mu \to \infty$). In that limit expression (14) becomes independent of fluxes and all events produce the same average power $\bar{\mathcal{P}}_0$. For other values of ν the spectral density is peaked at a power below $\bar{\mathcal{P}}_0$ (see fig. 5a).

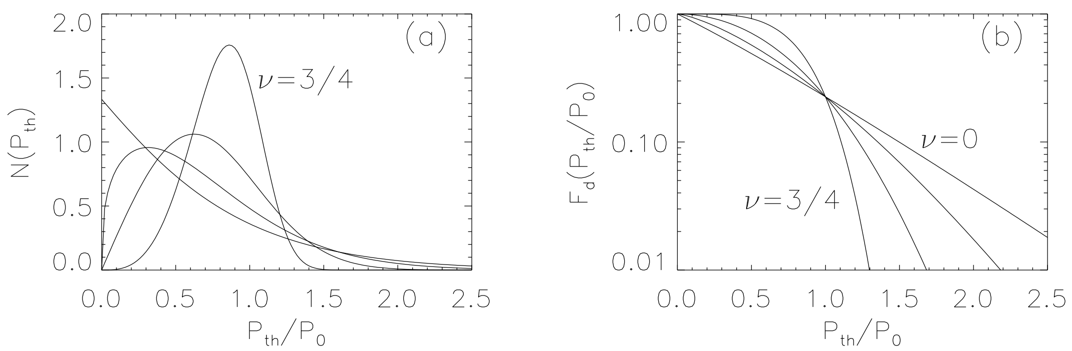

Fig. 5.— Reconnection events as functions of power for the cases $\nu = 0, \frac{1}{4}, \frac{1}{2}, \frac{3}{4}$. (a) Normalized density $\mathcal{N}(P)$. (b) The detection fraction $\mathcal{F}_{\rm d}(P_{\rm th}/\bar{\mathcal{P}}_0)$, giving the fraction of all events with average power above $P_{\rm th}$.

Consider an observation limited by a detection threshold $P_{\rm th}$; those events with $\bar{\mathcal{P}} < P_{\rm th}$ are not detected. In actual fact the visibility of an XBP depends more on the instantaneous power output than on the average power. Since the instantaneous power may vary erratically in response to the impulsive energy releases, we will work instead with the average power $\bar{\mathcal{P}}$. In such an observation, limited to $\bar{\mathcal{P}} \geq P_{\rm th}$, the number of detected XBPs per unit area is

$$\mathcal{D}(P_{\rm th}) = \int_{P_{\rm th}}^{\infty} \mathcal{N}(P)dP \ = \ \mathcal{D}_0 \, \mathcal{F}_{\rm d}(P_{\rm th}/\bar{\mathcal{P}}_0) \ \ , \tag{20}$$

where $\mathcal{D}_0 \equiv \mathcal{D}(P_{\rm th}\!=\!0)$ is the total density of reconnection events, and $\mathcal{F}_{\rm d}(x)$ is the detection fraction given by

$$\mathcal{F}_{\rm d}(x) \ \equiv \ (\,1 + \tfrac{2}{3}x^{\mu}\,)\, e^{-2x^{\mu}} \ \ . \tag{21}$$

If the detection threshold is at the nominal XBP power $P_{\rm th} = \bar{\mathcal{P}}_0$ then $\mathcal{F}_{\rm d}(1) = 22\%$ of the reconnection events are detectable, regardless of the velocity exponent ν (see fig. 5b).

4. Effect of the network

All of the foregoing calculations assumed the positive and negative magnetic elements to be distributed uniformly in space and independently of one another. The independence of the two distributions may be quantified using the two-point correlation of opposing flux elements. This property of the solar magnetic flux has not been measured yet, so we will not re-examine our assumption of independent distributions. The spatial distribution has, however, been studied and found to differ from uniformity. Flux elements are found preferentially along the magnetic network, coinciding with the lanes between supergranular cells. Concentrating the flux elements within subset of the surface is likely to increase the frequency of collisions. Thus we expect the results of the previous section to be systematically lower than corresponding results for elements distributed along the network. We will quantify this enhancement in a modified model for flux element interactions.

The magnetic network has been found to resemble the edges of a Voronoi tessellation (Schrijver *et al.* 1997a). Motivated by this observation we construct a model network by randomly distributing cell centers uniformly in space as a Poisson point process. The average density of this distribution is $1/\bar{S}$, where $\bar{S} \simeq 300\,{\rm Mm}^2$ is the average area of a supergranule (Hagenaar *et al.* 1997). The Voronoi cell about a given center consists of all points which are closer to that center than to any other. Figure 6a shows cell centers (+) distributed randomly, and the Voronoi cells they define (solid lines).

To distribute magnetic elements along this model network we proceed as follows. First, the elements are distributed uniformly, as before (e.g. fig. 1). Then each element is "swept" radially from its cell center onto the cell boundary. This results in a the modified spatial distribution of magnetic elements. As an example fig. 6b shows the result of sweeping the elements from fig. 1 to the boundaries of those cells in fig. 6a.

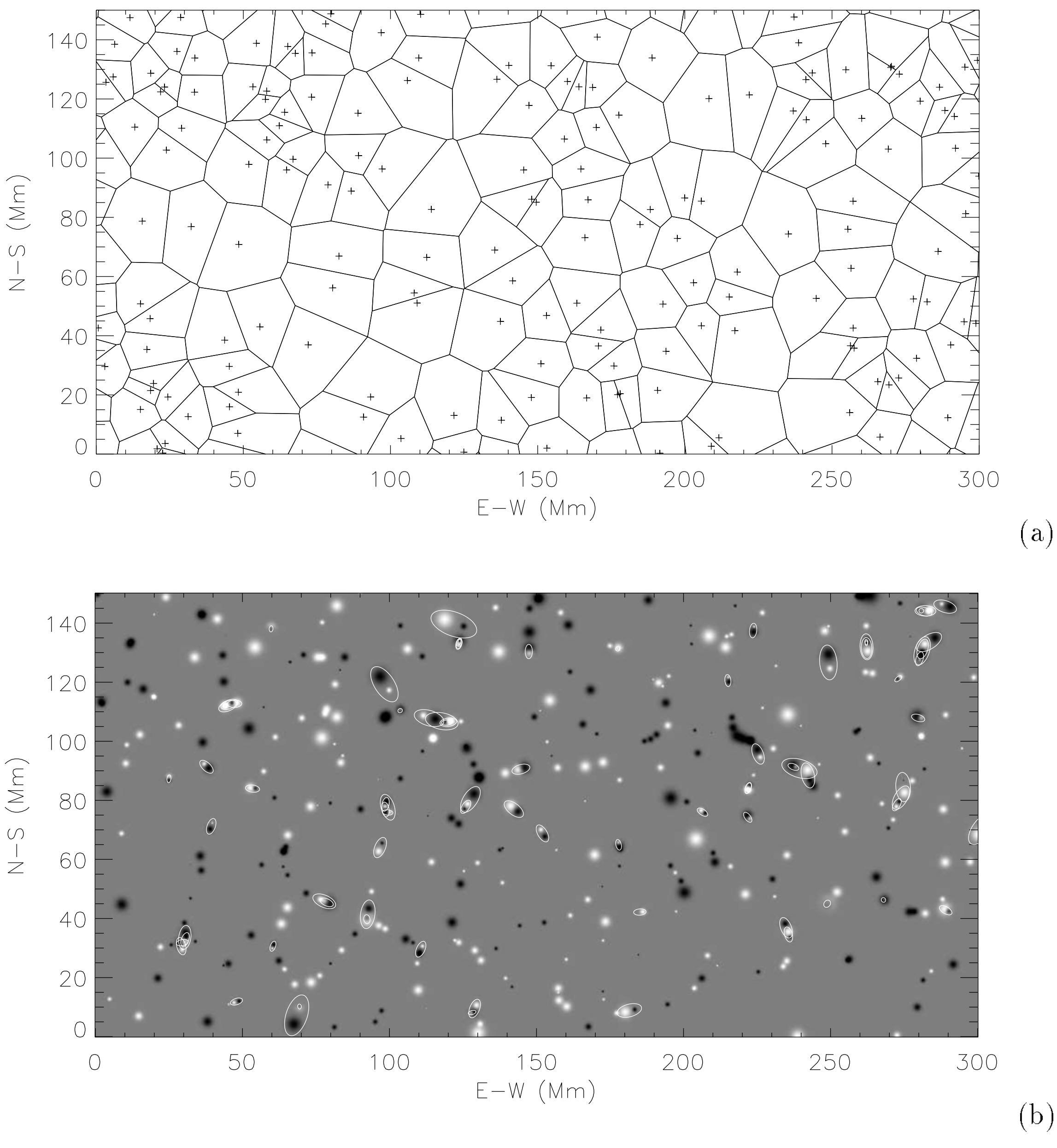

Fig. 6.— A model magnetic elements confined to the network. (a) The magnetic network (solid) resulting from uniformly distributed cell centers (+). The average cell area is $\bar{S} = 300\,\mathrm{Mm}^2$. (b) The magnetic elements from fig. 1 have been swept to the network. There are now 83 interacting pairs.

The spatial distribution of magnetic elements in this model is too complex to treat analytically. In order to proceed we will make the approximation that all interactions (collisions) occur between points on the same edge of a cell boundary. Since this amounts to concentrating all elements onto one dimension it would seem that this limit represents the most profound effect the network might have on interactions. In the opposite limit interacting elements are on the edges of different, widely separated cells. In this case it is hard to see how the "sweeping" has affected the interactions, other than to slightly displace each element in a random direction. Thus the case of uniform distribution corresponds to a limit of small network cells, while the "same-edge" approximation applies to the limit of large network cells.

After making the "same-edge" approximation a given pole Φ_+ will interact with opposing poles distributed, with some linear density, along a straight line. The average linear density must be proportional to the average surface density which has not been altered by the sweeping process. Similarly the the linear density per unit flux $\Lambda_-(\Phi_-)$ must be proportional to the corresponding surface density

$$\Lambda_-(\Phi_-) \ = \ \ell N_-(\Phi_-) \quad . \tag{22}$$

The constant of proportionality, ℓ, is defined so that the total length of network within a surface area A is A/ℓ (at least as $A \to \infty$). Statistical studies have shown that the average perimeter of a Voronoi cell is $4\bar{S}^{1/2}$ (Hinde and Miles 1980). Multiplying by the average number of cells per unit area, $\bar{S}^{-1}$, and then by $\frac{1}{2}$ (every element of network is on the perimeter of two cells at once) gives $\ell^{-1} = 2\bar{S}^{-1/2}$ or

$$\ell \ = \ \tfrac{1}{2}\bar{S}^{1/2} \ = \ 8.7\,\mathrm{Mm} \quad . \tag{23}$$

For comparison a square and an equilateral hexagon have perimeters $4\bar{S}^{1/2}$ and $3.72\bar{S}^{1/2}$ respectively. Therefore arrays of square or hexagonal super-granules would be characterized by $\ell = 0.5\,\bar{S}^{1/2}$ and $\ell = 0.54\,\bar{S}^{1/2}$.

In observations $\bar{S}^{1/2}$ is identified with the average "diameter" of a super-granule (by this logic ℓ is the average cell "radius".) Hagenaar *et al.*(1997) measured the average cell diameter to be 13–18 Mm (Hagenaar *et al.* 1997). Earlier measurements found values twice as large due to statistical biases inherent in the auto-correlation techniques used (Hagenaar *et al.* 1997).

The total number of interacting pairs follows from a generalization of the calculation leading to eq. (18). Considering negative poles in the flux range $(\Phi_-, \Phi_- + d\Phi_-)$, the average number which interact with a given positive pole is $2D(\Phi_+, \Phi_-)\,\Lambda_-(\Phi_-)\,d\Phi_-$. Integrating this over all positive and negative fluxes gives the density of XBPs

$$\begin{aligned}\mathcal{D}_0 &= \int_0^\infty d\Phi_+ N_+(\Phi_+) \int_0^\infty d\Phi_-\, 2D(\Phi_+,\Phi_-)\,\Lambda_-(\Phi_-) \\ &= (4-\sqrt{2})\Gamma(\tfrac{3}{2})\,\frac{\ell \bar{B}_+\bar{B}_-}{B_0^{1/2}\bar{\Phi}^{3/2}} \quad . \end{aligned} \tag{24}$$

Comparing this with expression (18) shows that the principle effect of the network is to increase the number of interacting pairs by the factor

$$\eta \;\equiv\; \frac{\ell B_0^{1/2}}{\bar{\Phi}^{1/2}} \;=\; \sqrt{\tfrac{1}{2}\bar{S}\beta B_0} \quad , \tag{25}$$

which is the ratio of a cell radius, ℓ, to a typical interaction distance $\sqrt{\bar{\Phi}/B_0}$. For the typical values $\eta = 3.7$ and the actual ratio between expression (18) and (24) is $1.8 \simeq \frac{1}{2}\eta$, in approximate agreement with the increase from 55 to 83 pairs between figs. 1 and 6b.

The same-edge approximation demands that $\eta \gg 1$ in order that the cell radius greatly exceed the typical interaction distance. Conversely, in cases where $\eta \ll 1$ the same edge approximation is invalid and expression (18) should be used in place of (24); in other words the network has no effect.

A similarly modified calculation yields the total heat flux from the network XBPs

$$\begin{aligned}F_{\rm XBP} &= \int_0^\infty d\Phi_+ \int_0^\infty d\Phi_-\, \mathcal{E}(\Phi_+,\Phi_-)\, 2V(\Phi_+,\Phi_-)\, N_+(\Phi_+)\,\Lambda_-(\Phi_-) \\ &= \eta\pi C'_\nu\, \alpha\, \bar{B}_-\bar{B}_+ v_0 \quad , \end{aligned} \tag{26}$$

where C'_ν is a numerical factor which varies smoothly between $C'_0 = 0.43$ and $C'_1 = 0.73$. Once again we find that confining elements to the network changes the corresponding result from a uniform distribution by the factor $\sim \frac{1}{2}\eta$.

5. Comparisons with published observations

The model above yields theoretical predictions for several measurable quantities which might be tested against published XBP studies. The model's predictions are expressed in terms of observable parameters of the photospheric field and its motion, $\bar{B}_\pm$, β and v_0. Unfortunately none of the published studies measured these quantities in conjunction with their observation of XBPs. Indeed, the best estimate of each parameter are the studies of quiet Sun regions already mentioned. In the absence of other data we are forced to apply the values $\bar{B}_\pm = 1.6$ G, $\beta = 0.3 \times 10^{-18}$ Mx and $v_0 = 200\,{\rm m/sec}$ to all quiet Sun regions.

Two other parameters, B_0 and α, characterize the magnetic reconnection. The parameter B_0 represents the typical background field strength in the vicinity of a colliding bipole. No attempt to has yet been made to more precisely define B_0, and until this is done it cannot be measured. Perhaps the best approach is to fit B_0 as a free parameter of the model. This may be best achieved in studies of XBP density, which we treat in the following subsection. We will show that $B_0 \simeq 30$ gives reasonable agreement with observation.

The other theoretical parameter, α, concerns the energetics of magnetic reconnection. The energy liberated by reconnection (in a quasi-static model) must scale as $B_0^{1/2}\Phi_<\Phi_>^{1/2}$ as in eq. (12); this can be seen by dimensional considerations alone. The constant of proportionality, α, relates to the details of the reconnection process, about which very little is known. It is possible to cast these details in terms of a threshold on the total current flowing in a singular layer along the separator. Longcope (1996) expressed the threshold current as a fraction θ of a current $I^\star$, which is characteristic of the potential field, and found $\alpha = 0.035\theta$. The current $I^\star$ is defined so that a sheet carrying this current has a width comparable to other global scales of the loop (e.g. its radius of curvature). A threshold value θ near unity therefore represents a current-sheet of global proportions. This has been used to argue that $\theta \lesssim 1$ (Longcope 1996). Since this has not been established using full MHD calculations, however, it is not an exact constraint on θ.

5.1. Energetics and heat flux

The best way to establish a value for θ would be to use either three-dimensional MHD simulations or detailed studies of XBPs (the latter is currently in progress.) The best study of XBP energetics from the existing literature is the rocket-born EUV survey by Kankelborg *et al.* (1996, 1997). This used snapshots at multiple wavelengths simultaneously to calculate instantaneous energy balance within each of 23 XBPs.(Kankelborg *et al.* 1997). The inferred heating powers ranged from 3×10^{23} ergs/sec to 3×10^{24} ergs/sec, with a median value of 10^{24} ergs/sec. Our model gives a theoretical expression for *average power* from an XBP

$$\bar{\mathcal{P}} \;=\; \alpha v_0 B_0 \Phi_< \;\simeq\; 2\times 10^{23}\,\theta\,(\Phi_</10^{19}\,\mathrm{Mx})\,\mathrm{erg/sec} \quad , \tag{27}$$

where we have assumed a relative footpoint velocity of $v_0 = 200\,\mathrm{m/sec}$ independent of flux (i.e. $\nu = 0$). Those XBPs which are nearest disk center and have median instantaneous power in the study (designated 2f and 3e in Kankelborg *et al.* 1997) occur at bipoles whose magnetic fluxes are found to be $\Phi_+ \simeq \Phi_- \simeq 3\times 10^{19}$ Mx. (This measurement was made using an archival KPNO line-of-sight magnetogram). Finally, comparing the interaction distance (6) to the measured loop lengths gives an estimate of the background field strength

$B_0 \simeq 10$–30 G.

Equating expression (27) with the observed power 10^{24} ergs/sec, and using observed fluxes yields the estimate $\theta \simeq 1$, It is encouaging that this observational estimate yields a threshold in keeping with our expectation that $\theta \lesssim 1$. Hereafter we will adopt this choice $\theta = 1$. An application of the MCC to a medium-sized compact flare (Longcope and Silva 1998) inferred a similar value.

The model above predicts a total heat flux given by expression (26), once the contentration of flux along the network is taken into account. Using $\theta = 1$ gives $F_{\rm XBP} = 1.4 \times 10^4\,{\rm ergs\,sec^{-1}\,cm^{-2}}$. This is a factor of three lower than the radiative losses from XBPs in the quiet Sun found by Habbal and Grace (1991). We consider this to be reasonable agreement considering that the most important factors in the heat flux, $\bar{B}_+$ and $\bar{B}_-$, are unmeasured. The next section will mention possible sources of additional heat, not included in our model. It should be noted that both predictions and the observations yield heat fluxes almost an order of magnitude too small to serve as the primary source of coronal heating.

5.2. XBP population

The model predicts a surface density of XBPs, given by eq. (24), which is $\mathcal{D}_0 = 2.3\eta\beta\bar{B}_+\bar{B}_-/B_0 \simeq 0.02$ per square Mm of surface. This would amount to an average of 4 events in a field of view one arcminute squared, near disk center. (Or $6,000$ events on the disk under the unlikely circumstance that the entire visible hemisphere were to be quiet Sun). An actual observation would detect only a fraction of these events as XBPs. The detected fraction would depend on spatial resolution, sensitivity, temperature response, level of background, and many other factors. We have attempted to account for some of these factors through a threshold $P_{\rm th}$ on average power. The fraction of events above the threshold is given by $\mathcal{F}_{\rm d}(P_{\rm th}/\bar{\mathcal{P}}_0)$.

Only a few studies have attempted a complete survey of XBPs suitable for measuring their surface density. Unfortunately, those studies did not report the magnetic quantities $\bar{B}_\pm$ or β, nor do they attempt to characterize their detection threshold. Habbal and Grace (1991) use *Skylab* images in several EUV wavelengths. In their 22.5 square arc-minute field of view ($5' \times 5'$ field-of-view with two small active regions removed) they identify ~ 12 XBPs. This gives a density of 0.5 per square arcminute. Porter *et al.* (1987) identify about two "network flares" in each $2' \times 2'$ C IV rasterized image from SMM. This leads to an estimate of 0.5 per square arcminute similar to Habbal and Grace 1991 (or 1,400 over the entire sun [Porter *et al.* 1987].) Both of these computed densities are about one-eigth of the predicted number of reconnection events $\mathcal{D}_0$. This could be explained by a detection threshold or $P_{\rm th} = 1.3\bar{\mathcal{P}}_0 \simeq 10^{23}\,{\rm erg/sec}$ for each of the instruments used.

The model also predicts the distribution of XBP powers, $\mathcal{N}(\bar{\mathcal{P}})$. This is a particularly powerful prediction, as it depends on only a single parameter $\bar{\mathcal{P}}_0$. Exploiting it, however, requires a survey of XBP powers which is *complete* above some lower limit $P_{\rm th}$. No such survey exists. To demonstrate the technique let us consider the the EUV study of Kankelborg *et al.* which calculated powers for each of 23 XBPs. All but one had power $\mathcal{P}_{\rm obs} > 5.8 \times 10^{23}\,{\rm ergs/sec}$. While this survey is not complete (nor did the authors ever intend it to be) the data suggests that above 5.8×10^{23} ergs/sec, the sampling may be fairly representative (i.e. excluding the single XBP [3b in Kankelborg *et al.* 1997] with $\mathcal{P}_{\rm obs} = 3 \times 10^{23}$ ergs/sec).

Figure 7 shows a normalized cumulative histrogram of those data with $\mathcal{P}_{\rm obs} \geq 5.8 \times 10^{23}$ ergs/sec. Assuming the sampling is complete, fig. 7 shows the fraction of XBPs with $\bar{\mathcal{P}} > P_{\rm th}$ *which also* have $\bar{\mathcal{P}} > P$. The theoretical expression for this quantity is

$$\text{Fraction of observed XBPs with } \bar{\mathcal{P}} \; > \; P \quad = \quad \frac{\mathcal{D}(P)}{\mathcal{D}(P_{\rm th})} \; = \; \frac{\mathcal{F}_{\rm d}(P/\bar{\mathcal{P}}_0)}{\mathcal{F}_{\rm d}(P_{\rm th}/\bar{\mathcal{P}}_0)} \quad , \tag{28}$$

where we have taken $\nu = 0$ ($\mu = 1$) in fig. 7. This expression depends only on $\bar{\mathcal{P}}_0$ since $P_{\rm th}$ is fixed when constructing the histrogram. Curves from (28) are plotted for values from $\bar{\mathcal{P}}_0 = 10^{23}\,{\rm ergs/sec}$ ($\diamond$) to $\bar{\mathcal{P}}_0 = 3 \times 10^{24}\,{\rm ergs/sec}$ ($*$). For $\bar{\mathcal{P}}_0 = 10^{24}\,{\rm ergs/sec}$ ($\triangle$) expression (28) fits the data very well (the Kolmogorov-Smirnov D is 0.07). This can be reconciled with previous results, (e.g. $\theta = 1$), if for example $\bar{\Phi} = 5 \times 10^{19}$ Mx, while B_0 retains its former values of 30 G. This value of $\bar{\Phi}$ is an order of magnitude larger than the quiet sun observations of Schrijver *et al.*(1997).

Let us assume for the moment that the quiet sun of May 13, 1991 (soon after solar maximum) was in fact characterized by $\bar{\Phi} = 5 \times 10^{19}$ Mx. The surface density of reconnection events would then be $\mathcal{D}_0 = 10^{-4}\,{\rm Mm}^{-2}$ (note that the new $\bar{\Phi}$ leads to $\eta = 0.87$, implying that the network is only partially significant). At the moment of observation roughly half of the visible disk is quiet Sun, so there would be 150 reconnection events. Of these the model predicts that $150\,\mathcal{F}_{\rm d}(0.58) = 64$ would have $\bar{\mathcal{P}} > 0.58\bar{\mathcal{P}}_0 = 5.8 \times 10^{23}\,{\rm erg/sec}$. This is about three times as many as listed in their study. Based on a visual inspection of the images in Kankelborg *et al.* (1997), it does not seem unreasonable that their incomplete survey includes one of every three XBPs. Note that at the surface densities *observed* by Habbal and Grace (1991) there should have been 800 XBPs in th quiet sun (occupying $\sim \frac{1}{2}$ the disk), of which Kankelborg *et al.* report on only 23.

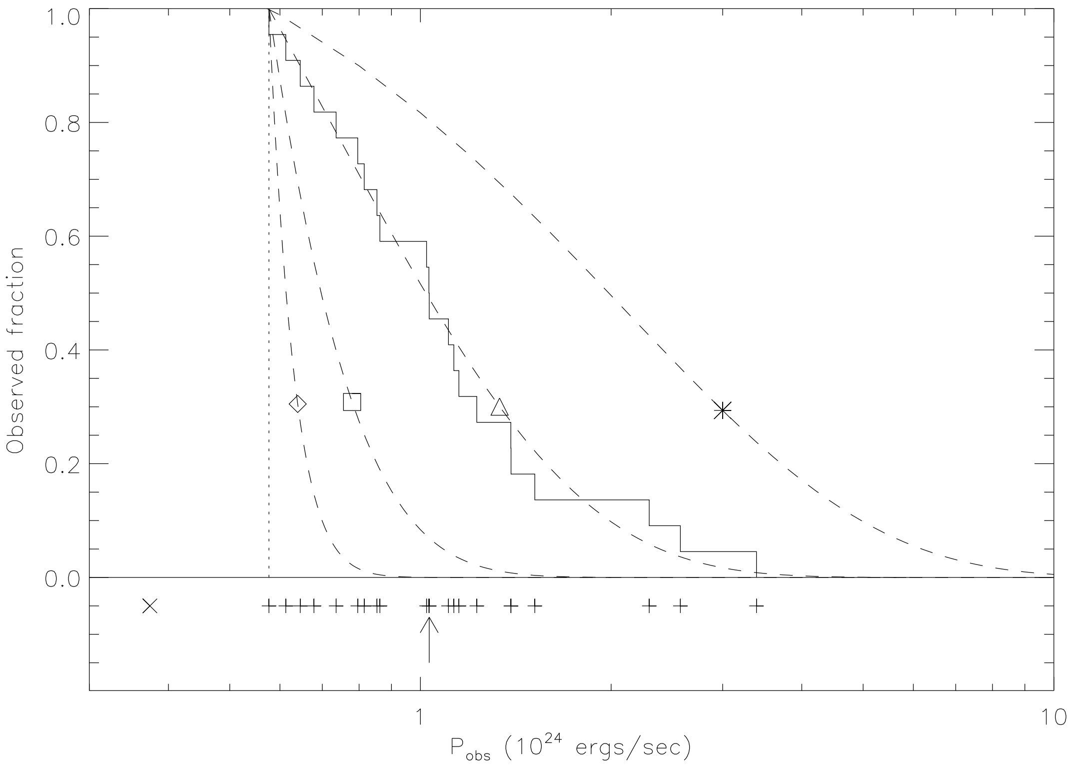

Fig. 7.— The cumulative histogram of XBP power from observation of Kankelborg *et al.* 1997 (solid). The abscissa gives $\mathcal{P}_{\rm obs}$ in units of 10^{24} ergs/sec. Data points from the 23 XBPs are indicated by $+$'s and $\times$'s along the bottom, with an arrow indicating the median power 10^{24} ergs/sec. (The $\times$ marks a single data point excluded from the histrogram). The completeness threshold, $P_{\rm th} = 5.8 \times 10^{23}$ ergs/sec, used to calculate the histrogram is indicated by a dotted vertical line. Theoretical predictions, eq. (28), are shown by dashed lines for choices $\bar{\mathcal{P}}_0 = 10^{23}$ ergs/sec ($\diamond$), $\bar{\mathcal{P}}_0 = 3 \times 10^{23}$ ergs/sec ($\Box$), $\bar{\mathcal{P}}_0 = 10^{24}$ ergs/sec ($\triangle$), and $\bar{\mathcal{P}}_0 = 3 \times 10^{24}$ ergs/sec ($*$).

6. Discussion

We have developed a model for the coronal response to the interaction of randomly moving photospheric elements. In the model the collision between two elements of opposing signs results in reconnection and the appearance of an XBP. A section of quiet sun on which elements are distributed and moving at random, will contain a number of XBPs. The model yields quantitative predictions for the surface density of XBPs, their distribution of luminosities, and their contribution to the total heat flux in the quiet sun. The model combines three basic ingredients: 1. a distribution of element sizes, 2. rms velocities of elements, 3. a model for a pair-wise collision, including interaction distance and energy release. The quantitative results depend to varying degrees on each of the ingredients.

6.1. The model ingredients

The flux-distribution has been assumed to be exponential of the form (1) with parameters $\bar{B}_{\pm}$ and β taken from a single study of the quiet sun (Schrijver *et al.* 1997c). The few observational studies which measure the element flux distributions generally agree on a decreasing spectral form. The choice of an exponential spectrum led to closed-form results from which dependencies could be readily extracted. The same parameters can be defined from moments of arbitrary distribution functions

$$\bar{B}_{\pm} \equiv \int_0^\infty \Phi\, N_{\pm}(\Phi)\, d\Phi \quad , \tag{29}$$

$$\beta_{\pm} \equiv \langle\Phi_{\pm}\rangle^{-1} = \bar{B}_{\pm}^{-1} \int_0^\infty N_{\pm}(\Phi)\, d\Phi \quad . \tag{30}$$

(The analysis would then need to be generalized to use different values of β for each species.) Results from this generalized model would then scale exactly as those in §3, but with different numerical factors.

The root-mean-squared velocity is assumed to depend weakly on flux in eq. (4) as indicated by observational studies (Schrijver *et al.* 1996). Flux dependence is introduced though the exponent ν, which is found not to greatly affect the results of the model. Measurements of $v_{\rm rms}$, however, show a dependence on flux which is not singular as $\Phi \rightarrow 0$. A better model to fig. 10 in Schrijver *et al.* 1996 would take the form

$$v_{\rm rms}(\Phi) \simeq u_0 - u_{-1}\,(\beta\Phi) \quad , \tag{31}$$

where $u_0 \simeq 260$ m/sec and $u_{-1} \simeq 60$ m/sec, so that $v_{\rm rms}(\bar{\Phi}) = v_0 = 200$ m/sec. This was not used in work above because it is more cumbersome and because it suffers from the more serious defect that $v_{\rm rms} < 0$ over some range. Nevertheless, using this in expression (15) gives

$$F_{\rm XBP} = \pi\alpha\bar{B}_+\bar{B}_-\,(C_0 u_0 \;-\; C_{-1}u_{-1}\,) \;\simeq\; 0.5\times10^4\,{\rm erg\,sec^{-1}\,cm^{-2}} \;\;, \tag{32}$$

where $C_0 = 1$ and $C_{-1} = \frac{5}{4}$. This is barely different from the previous $\nu = 0$ result, demonstrating once again the small affect of velocity flux-dependence.

The model for pair-wise collisions is taken from the minimum current corona model (Longcope 1996, Longcope 1998). The MCC model concerns only the reconnection of coronal field lines between isolated photospheric features. It neglects all other processes, including many potentially significant contributions. It is generally conceded, based on observations, that reconnection does occur between magnetic features. The strength of the MCC is that it quantifies the energetic contribution of that process *in the absence of all others*. The success or failure of foregoing model, in the face of observations, will clearly indicate how significantly reconnection actually contributes to the corona.

6.2. Coronal heat flux

The most notable prediction of the model is the heat flux due to magnetic reconnection events (i.e. eq. [15])

$$F_{\rm XBP} \;=\; \pi C_\nu\,\alpha\,\bar{B}_-\bar{B}_+ v_0 \;\;, \tag{33}$$

where we have here ignored the effects of the network in the interest of clarity. This simple expression depends on general aspects of the model's three ingredients, but *not* on the details of these ingredients. The quasi-static nature of the energy release model demands the linear dependence on photospheric velocity v_0. Furthermore, since heat is generated by collisions the expression is proportional to the surface density of each species of collider. It is assumed that only those collisions between opposing polarities produce heat, so the heat flux is proportional to the product $\bar{B}_+\bar{B}_-$. These plausible assumptions lead immediately to expression (33) on dimensional grounds alone. The numerical coefficient $\pi C_\nu\alpha \simeq 0.1$ does depend on the details of the models: for example C_ν comes from the double integral over the exponential size distributions.

Expression (33) differs from other coronal heating models in several notable respects. For example, fluxes from wave heating models are always quadratic in v_0 (Hollweg 1990) since that is the velocity-scaling for Alfvén wave energy. The direction of a magnetic field line has no effect on Alfvén waves, so wave heating models depend on the total unsigned flux, rather than on a product of the densities of each polarity. In particular, a unipolar portion of the surface can be effectively heated by waves, while it cannot be heated by reconnection between opposing flux elements (expression [33] vanishes for unipolar regions).

Expression (33) also differs from comparable expressions in many DC heating models, where heat flux scales quadratically in both normal magnetic field and velocity (Sturrock and Uchida 1981, Parker 1983, Van Ballegooijen 1986, Parker 1988). The quadratic dependence on velocity in these quasi-static models results from parameterizing reconnection by a "reconnection time". Were this time to be written as a critical distance divided by the velocity, the expression would become linear in velocity. Indeed, some DC models begin by parameterizing reconnection by a displacement or twist angle, rather than a time, and do find heating rates linear in velocity (Browning *et al.* 1986, Longcope 1996).

Moreover, DC heating models are typically proposed for active regions, whereas the model presented here is for the quiet sun. Magnetic interactions in active regions are much more complex than the simple binary collisions treated in this model. We thus do not expect the generic DC heat flux to depend simply on a product of the flux density in each polarity.

As a quasi-static model, the MCC is distinct from AC heating models in a clear sense: it scales as v_0 in the limit $v_0 \to 0$. According to this distinction, certain theoretical manifestations of magnetic reconnection, such as X-point collapse (Hassam 1992, Craig and McClymont 1993), are classified as AC and are therefore neglected by our model. Using heating estimates based on the MCC quantifies the contribution of DC heating alone.

The MCC includes only reconnection *between* flux elements and neglects reconnection *within* a flux element. The magnetic equilibria used to calculate $\mathcal{E}$ are not subject to full line-tying constraints. For example, a constraint is placed on the number of field lines (i.e. total flux) which connect P to N in fig. 2, but *no constraint* is placed on how those field lines are connected. The field is therefore free to assume a potential solution within the P–N flux system, and current in the MCC model flows only *between* flux systems. One immediate consequence of this is that the field cannot be stressed by twisting one of the footpoints; this kind of energy is neglected in MCC. This is a convenient thing to neglect since understanding twist requires a model for the internal structure and velocity of the flux tube. Dynamical flux tube theories (Spruit 1981) are not applicable at the photospheric layers, nor do our best observations (Schrijver *et al.* 1997c) reveal much about the internal structure of magnetic features.

Finally, no energetic contributions from the chromosphere are included. There are several theoretical studies of reconnection at this level (Ryutova *et al.* 1997), but we have not included these. Once again our motivation was to develop a model which includes a single physical process, in order to assess the significance of this process. The detailed structure of the magnetic field at the chromosphere is poorly understood, and the reconnection there is likely to be much more complex than reconnection in the corona.

The total heat flux predicted by our model falls well short of the amount thought to be heating the quiet sun corona, $F \simeq 3 \times 10^5\,\mathrm{erg\,cm^{-2}\,sec^{-1}}$ (Withbroe and Noyes 1977). *Based on our model, magnetic reconnection cannot be the primary source of coronal heating in the quiet Sun.* This might be one more case in which impulsive reconnection events fail to fulfill the role of a steady-state coronal heating mechanism. Another well-known case is that of micro-flares and nanoflares, whose energetic contributions has been estimated (Hudson 1991), and found to be inadequate. Observational estimates of the contribution of XBPs have shown them to be similarly inadequate (Habbal and Grace 1991). The remaining heat must come from one of the energetic contributions excluded from our model e.g. Alfvén waves, reconnection within bipoles, or from energies related to interactions more complex than binary collisions.

Comparisons of this model to published observations are extremely encouraging. Predictions of total heat flux, surface density and the spectral distribution of XBPs are close to observed values. Unfortunately, all of these comparisons suffer from a lack of data. The model predictions depend on three magnetic parameters, $\bar{B}_+$, $\bar{B}_-$, β, as well as on v_0. Furthermore, the predictions concern the complete population of XBPs. A full test of the model requires a survey of XBPs which is complete to some observational limit, combined with measurements of these photospheric parameters.

The authors wish to acknowledge helpful discussions with Dr. C. J. Schrijver, and to thank the anonymous referee for helpful comments on the manuscript. This material is based upon work supported by the National Science Foundation under Grant No. ATM-9733424. C.C.K. was supported under grant NAG5-7296.

References

Browning, P. K., Sakurai, T., and Priest, E. R. (1986). *A&A* **158**, 217.

Craig, I. J. D. and McClymont, A. N. (1993). *ApJ* **405**, 207.

Dennis, B. R. (1985). *Solar Phys.* **100**, 465.

Gabriel, A. H. (1976). *Phil. Trans. R. Soc. Lond.* **A281**, 339.

Habbal, S. R. and Grace, E. (1991). *ApJ* **382**, 667.

Hagenaar, H. J., Schrijver, C. J., and Title, A. M. (1997). *ApJ* **481**, 988.

Harvey, K. L., Nitta, N., Strong, K. T., and Tsuneta, S. (1994). In Uchida, Y., Watanabe, T., Shibata, K., and Hudson, H. S., editors, *X-ray solar physics from Yohkoh*, pp. 21–24.

Universal Academy Press.
Hassam, A. B. (1992). *ApJ* **399**, 159.
Hinde, A. L. and Miles, R. E. (1980). *Statist. Comput. Simul.* **10**, 205.
Hollweg, J. V. (1990). *Comp. Phys. Rep.* **12**, 205.
Hudson, H. S. (1991). *Solar Phys.* **133**, 357.
Kankelborg, C. C., Walker, II, A. B. C., and Hoover, R. B. (1997). *ApJ* **491**, 952.
Kankelborg, C. C., Walker, II, A. B. C., Hoover, R. B., and Barbee, T. W., J. (1996). *ApJ* **466**, 529.
Kendall, M. G. and Moran, P. A. P. (1963). *Geometrical probability.* Griffin's Statistical Monographs. Charles Griffin and Co., London.
Lin, R. P., Schwartz, R. A., and Kane, S. R. (1984). *ApJ* **283**, 421.
Longcope, D. W. (1996). *Solar Phys.* **169**, 91.
Longcope, D. W. (1998). *ApJ* **507**, 433.
Longcope, D. W. and Cowley, S. C. (1996). *Phys. Plasmas* **3**(8), 2885.
Longcope, D. W. and Silva, A. V. R. (1998). *Solar Phys.* **179**, 349.
Parker, E. N. (1983). *ApJ* **264**, 635.
Parker, E. N. (1988). *ApJ* **330**, 474.
Porter, J. G., Moore, R. L., Reichmann, E. J., Engvold, O., and Harvey, K. L. (1987). *ApJ* **323**, 380.
Priest, E. R., Parnell, C. E., and Martin, S. F. (1994). *ApJ* **427**, 459.
Ryutova, M., Schrijver, C. J., Shine, R. A., Tarbell, T., Berger, T., and Title, A. M. (1997). In DeLuca, E. E. and Bookbinder, J., editors, *Proceedings of the High Resolution Solar Atmospheric Dynamics Workshop.* In press.
Schrijver, C. J., Hagenarr, H. J., and Title, A. M. (1997a). *ApJ* **475**, 328.
Schrijver, C. J., Shine, R. A., Hagenaar, H. J., and Hurlburt, N. (1996). *ApJ* **468**, 921.
Schrijver, C. J., Title, A. M., Hagenaar, H. J., and Shine, R. A. (1997b). *Solar Phys.* **175**, 329.
Schrijver, C. J., Title, A. M., Harvey, K. L., Sheeley, N. R., J., Wang, Y.-M., van den Oord, G. H. J., Shine, R. A., Tarbell, T. D., and Hurlburt, N. E. (1998). *Nature* **394**, 152.
Schrijver, C. J., Title, A. M., Van Ballegooijen, A. A., Hagenaar, H. J., and Shine, R. A. (1997c). *ApJ* **487**, 424.
Spruit, H. C. (1981). *A&A* **98**, 155.
Sturrock, P. A. and Uchida, Y. (1981). *ApJ* **246**, 331.
Van Ballegooijen, A. A. (1986). *ApJ* **311**, 1001.
Webb, D. F., Martin, S. F., Moses, J. W., and Harvey, J. W. (1993). *Solar Phys.* **144**, 15.
Withbroe, G. L. and Noyes, R. W. (1977). *ARA&A* **15**, 363.
Zwaan, C. (1987). *ARA&A* **25**, 83.

This preprint was prepared with the AAS LaTeX macros v4.0.